Presented at the Symposium on High Spin
Phenomena in Nuclei, Argonne, France,
March 15-17, 1979

LBL-8965
CONF-790323--4

NUCLEAR STRUCTURE FROM CONTINUUM γ-RAYS

R. M. Diamond

MASTER

March 1979

Prepared for the U. S. Department of Energy
under Contract W-7405-ENG-48

LAWRENCE BERKELEY LABORATORY
UNIVERSITY OF CALIFORNIA
BERKELEY

NUCLEAR STRUCTURE FROM CONTINUUM γ-RAYS

R. M. Diamond

Lawrence Berkeley Laboratory
University of California
Berkeley, California 94720

NOTICE
This report was prepared as an account of work sponsored by the United States Government. Neither the United States nor the United States Department of Energy, nor any of their employees, nor any of their contractors, subcontractors, or their employees, makes any warranty, express or implied, or assumes any legal liability or responsibility for the accuracy, completeness or usefulness of any information, apparatus, product or process disclosed, or represents that its use would not infringe privately owned rights.

The meaning of the words high spin, like heavy ion, depends upon the person using them. For those who work with light nuclei, spins of 8 or 10 are high. For decay-scheme spectroscopists, spins of 20 are high. I want to discuss with you the properties of states of spin 20-60. Why stop at 60? Nature provides a limit where the fission barrier vanishes, and an estimate of this limit is furnished by the liquid-drop model.[1] This is shown as the upper full line in Fig. 1. Actually, fission still occurs with small barriers, and so the dashed line in the figure gives the lower more realistic spin limit corresponding to a barrier of 8 MeV. This curve reaches a maximum of ~75 at A=120. Alpha-particle emission may set even lower limits,[2] especially for nuclei with A< 120, and neutron evaporation carries off some spin, so the angular momentum finally available for the γ-ray de-excitation cascade is somewhat lower still.

What else can the liquid-drop model tell us? If we assume that quadrupole deformation is the lowest deformation mode of the drop, then under rotation the drop will become oblate with its symmetry axis along the rotation axis. But somewhat higher-lying states can exist for other shapes. If, for simplicity, we restrict ourselves to axially symmetric shapes (not that nature will), there are four cases: oblate or prolate shape, and rotation axis parallel or perpendicular to the symmetry axis. For rigid rotation with a definite value of $\beta \approx \Delta R/R$, the moments of inertia of these four cases can be expressed in terms of the moment of inertia of a rigid sphere, $\mathcal{J}_0$, as shown in Fig. 2. These moments lead to the rotational state trajectories also shown, with the oblate-parallel case lowest as it has the largest moment of inertia.

For real nuclei, there are two additional considerations. The first is shell effects, which are of order 3-8 MeV, and favor one or another of the cases depending upon the particular nucleon orbits near the Fermi surface. For $I < 30$, shell effects are large compared to the differences in energy of the four systems, and thus they dominate the determination of the shape and the nature of the excitation. But for $I > 40$, the differences in the liquid-drop energies may dominate, and one might expect to find mainly oblate shapes rotating around the symmetry axis or prolate shapes rotating about an axis perpendicular to the symmetry axis.

However, the second consideration is that real nuclei are not classical, but are small, quantal systems. Rotation about an axis perpendicular to the symmetry axis is allowed, and corresponds to collective rotation,[3] that is, to bands with transition energies proportional to the spin $(E_\gamma = \hbar^2/2\mathcal{J}(4I-2))$ and with strongly enhanced B(E2) values. Most known rotational nuclei are of this type. But collective rotation around the symmetry axis cannot occur quantum-mechanically, so what about the oblate case with such rotation as favored by the liquid-drop calculations? Bohr and Mottelson[4] have pointed out that the angular momentum can be carried by individual high-j nucleons aligned along the symmetry axis, rather than by the nucleus as a whole, and so it is not a collective motion. But now there is no correlation between transition energy and spin, and no enhanced B(E2) values. However, they showed that for a Fermi-gas distribution the energies of the yrast states followed, on the average, the classical curve of Fig. 2.

Now let us apply these ideas to what we might expect in the γ-ray de-excitation of nuclei formed at very high (up to 60 $\hbar$) angular momenta in (H.I.,xnγ) reactions. Figure 3 shows a plot of excitation energy vs. angular momentum for a nucleus with $A \sim 160$. The heavy solid line indicates schematically the range of angular momentum populated in such a nucleus following an (^{40}Ar,4n) reaction. Regions of lower spin give mainly 5n products, and the spins just above yield a small amount of 3n product. This fractionation of products by angular momentum means that the highest spin states are in the product involving the smallest number of evaporated neutrons. Several types of γ-ray transitions appear in

the subsequent de-excitation of such a nucleus. There are "statistical" transitions that carry off energy and little angular momentum, bringing the nucleus towards the yrast line. There may be collective E2 transitions that form bands parallel to the yrast line, carrying off two units of spin apiece as well as energy. There are many pathways, so that no single transition has enough intensity to stand up in the spectrum; this leads to the name, "continuum" γ-ray spectrum. When the nucleus cools to the region of the yrast line, at spins between 10 $\hbar$ and 40 $\hbar$ depending upon the type of nucleus, then enough population goes through the individual transitions to make them visible in the spectrum as resolved or discrete lines, the usual goal of γ-ray spectroscopists.

We believe that the statistical transitions do not depend very much on the nuclear structure, but we have earlier discussed that the existence of collective rotational transitions do depend strongly on the type of nucleus. For a prolate nucleus (or triaxial nucleus favoring prolate shape) rotating around an axis perpendicular to the symmetry axis, the rotational bands favor decay roughly parallel to the yrast line, and so lead to low spins before sufficient cooling takes place to allow observation of the discrete lines ($\sim$20 $\hbar$). On the other hand, oblate nuclei (or triaxial nuclei of dominantly oblate shape) rotating around their symmetry axis have their collective transitions suppressed, and so de-excite more steeply into that line. Thus it is reached at a higher spin, and since in this case it is irregular, being composed of single-particle states, not only are discrete states of higher spin observable, but some may be long-lived enough to become isomers.

It now appears that both of these types of behavior are observed experimentally. In the regions just above N=82 or 126, states with spins as high as 37 have been seen in the de-excitation cascades from (presumably oblate) reaction products,[5,6] and these will be discussed in later talks. In the remainder of my talk, I shall concentrate on the prolately deformed nuclei leading to collective rotational de-excitation cascades that generally do not show discrete transitions until below spins of 20-30 $\hbar$. Thus, all the information we are likely to obtain about the high-spin states must come from studies of the continuum. Figure 4 shows an example of the de-excitation

cascades from the 4n product of 181 MeV $^{40}Ar + ^{126}Te \rightarrow ^{166}Yb^*$, taken with a 7.6 × 7.6 cm NaI detector in coincidence with a Ge detector gated on the 4n lines.[7] The value of ℓ_{max} in the reaction is ~75, but fission and transfer reactions take off the highest spins, and the four neutrons carry off a few units more of angular momentum, so that the maximum spin of the highest states in this γ-ray cascade correspond to about 60 ħ. The open squares are the raw pulse-height spectrum, and one can distinguish the high-energy exponentially-falling statistical tail and the lower-energy (below 1.5 MeV) yrast bump. The filled points are the same spectrum unfolded, that is, corrected for the NaI response function, to yield the primary γ-ray spectrum, and divided by the NaI efficiency and the number of singles in the Ge counter to yield the absolute number of transitions per event per 40 keV interval. The sum of these points is ⟨M-1⟩, the average multiplicity minus the one trigger γ-ray in the Ge detector (⟨M⟩ ≈ 24 in this case). The angular anisotropy of the γ-rays is shown at the top of the figure. The large anisotropy observed between 800-1400 keV, the region of the yrast bump, indicates almost pure stretched E2 transitions in that bump. The isotropy above 2 MeV permits little to be said about the multipolarity of the high-energy statistical transitions (but see below), and there is also a decrease towards unity at low transition energies. In fact, the anisotropy falls below unity for $E_\gamma < 500$ keV in some nuclei. The high-energy statistical tail is very similar in a number of nuclei, and for a number of bombarding energies, while the bump differs from nucleus to nucleus and with bombarding energy. An example of the latter situation is shown at the bottom of Fig. 4. The solid line is the locus of the unfolded points above for 181 MeV ^{40}Ar bombardment. The dotted, short-dashed, and long-dashed lines are similar representations of the continuum spectra from the reactions (331 MeV) $^{86}Kr + ^{80}Se$, (87 MeV) $^{16}O + ^{150}Sm$, and (157 MeV) $^{40}Ar + ^{126}Te$, respectively, to yield ^{162}Yb + 4n. These three reactions involve about the same average angular momentum (25-30 ħ) in the γ-ray cascade of the ^{162}Yb product, and the spectra are almost identical. In contrast, the higher energy (181 MeV) ^{40}Ar reaction brings more angular momentum to the cascade (~40 ħ on average), and the additional γ-rays de-exciting these higher-spin states move the edge of the bump to higher transition energy. This is in agreement with the

idea that these γ-rays are members of collective bands running roughly parallel to the yrast line, as such rotational transitions have energies proportional to the spins of the initial states. The lower-energy part of the bump (lower-spin rotational transitions) and the statistical transitions are not much affected by the increased angular momentum. Figure 5 shows similar plots for other reaction channels of $^{40}Ar + ^{126}Te$, with similar results. At either a higher energy or a fewer-neutron-out channel, there is more angular momentum to be removed by the collective rotational cascades making up the bump, and its edge, representing the transitions from the states of highest spin, moves to higher transition energies. If we also knew the spins of these highest states, we could determine their effective moments of inertia from the rotational formula, $E_\gamma = \hbar^2/2\mathcal{J}(4I-2)$. We can, in fact, estimate the spins from the multiplicities, $\langle I \rangle = 2(\langle M \rangle - \delta)$ where $\delta = 3-4$ is the number of statistical γ-rays assumed to carry out no spin, and the rest of the γ-rays are stretched E2 transitions in the case of a good rotor. There are also other ways to estimate the moments of inertia of these continuum high-spin states, and all methods yield values within 10-20% of the rigid-sphere numbers. They are usually larger, suggesting deformation, but this is within the range of errors, both experimental and theoretical. However, just from the shapes (and changes in shape) of these spectra alone, we have thus obtained an indication of rotational bands, the average multiplicities, and estimates of the moments of inertia at high spin.

By their very nature, continuum γ-ray measurements are not as precise and as unambiguous as discrete line studies. So a variety of techniques must be used to get as many different types of insight on the nature of the continuum states and transitions as possible. For example, the isotropy of the high-energy tail of the continuum spectrum yields little information on the multipolarities involved. But recent measurements of conversion-electron coefficients of the continuum have given very specfic results,[8] namely, the high-energy transitions are almost pure E1 (Fig. 6). The two cases studied do not make a complete story, but if this result is generally true, the usually observed angular isotropy for these transitions requires that they be a 1/3-2/3 mixture of $\Delta I=0$ and $\Delta I=1$ electric dipoles, and so for good rotors this would

leave uncertain only the multipolarities of the low-energy transitions.

A quite different, but very useful technique, is to measure the average γ-ray multiplicity as a function of transition energy.[2,9] Because the multiplicity is related to the spin of the nucleus, any structure in the spectrum gives information on γ-ray energy — spin correlations in the continuum. Examples of three target-projectile systems at several bombarding energies are shown on the left in Fig. 7. For $^{40}Ar + ^{124}Sn \rightarrow ^{164}Er^*$, there is a pronounced peak in the multiplicity spectrum, and it comes at the edge of the bump in the intensity spectrum, corresponding to the highest-energy and highest-spin transitions. This peak moves to higher energy with increasing bombarding energy. Such a correlation is a nice confirmation of the collective rotation picture for this nucleus. Away from the deformed rotators, however, there may be more complex, hence more interesting, behavior. The $^{40}Ar + ^{82}Se \rightarrow ^{122}Te^*$ system (middle of Fig. 7), for example, does not show a rotational peak at 121 and 131 MeV, but develops it at still higher bombarding energies and angular momenta ($\ell_{max} > 30$). That is, the initially near-spherical ^{118}Te, whose ground state band has roughly equidistant levels, deforms to a rotor only above spin 35. The $^{48}Ca + ^{100}Mo \rightarrow ^{148}Sm^*$ system shown at the bottom of the figure is the most striking example we have found; the nearly semi-magic product nuclei do not show formation of a rotational peak until about spin 50, a very different situation from that with the ^{124}Sn target.

Still another helpful type of information comes from measurement of the average lifetimes in the yrast bump region of the continuum spectra. This can be done by comparing the Doppler-shift using a thin target with that from a gold- or lead-backed target.[10] To increase the magnitude of the effect, an inverse reaction is used, i.e., Xe projectiles are used to bombard an Al target, resulting in ^{163}Ho compound nuclei with Doppler shifts of 8 to 9%. The two spectra can be normalized to each other at transition energies above 2 MeV, and the raw pulse-height spectra are shown at the top of Fig. 8. The differences appear quite small, but are magnified when the thin target spectrum is divided, channel-by-channel, by the backed target one, as shown in Fig. 8b for the raw data and in Fig. 8c for the unfolded spectra. The analysis involves assuming a rotational cascade decay along the yrast region and

depends upon a single parameter, the constant intrinsic quadrupole moment, Q_o, of the deformed nucleus, or alternatively, the corresponding enhancement factor over single-particle decay. The value of this parameter is obtained from the best fit to the ratio of the unfolded spectra, and is shown in Fig. 8c as a solid curve. The enhancement factors found with ^{163}Ho and ^{164}Er compound nuclei were of the order of 300 ± 100, showing that in the spin range 30-50 ħ these nuclei (already deformed in their ground bands) decay through strongly enhanced, hence deformed, rotational bands.

Finally, I would like to mention a promising new technique for selecting a narrower band of angular momentum at high spin than can be done by choosing a reaction channel or by using a multiplicity filter, and indicate what can be done with this better selection. The method is to measure the total γ-ray energy by placing the target inside a large NaI spectrometer which is in coincidence with another detector,[11] and then observe the variation in the spectrum of the latter counter for different energy "slices" in the sum spectrometer. We used a 33 cm × 20 cm NaI crystal, divided optically into four sectors, and with a 2.9 cm hole along the axis to bring the beam into the target and to provide an opening from the target to either a coincident Ge or 7.6 cm × 7.6 cm NaI detector placed 11 cm or 60 cm away along the beam axis.[12] From the ratio of coincidences to singles for each "slice" of summed energy (including the outside NaI counter), γ-ray multiplicities could be determined as a function of the (slice) total γ-ray energy, and these are plotted in Fig. 9 for ~3 MeV wide slices for the reaction 185 MeV ^{40}Ar + ^{124}Sm → ^{164}Er*. It is clear that there is a strong correlation between γ-ray multiplicity and sum energy (at least for good rotors, as in this case).

When an array of six NaI counters at 120 cm from the target were substituted for the single one, the ratios of the zero-, first-, and second-fold counts gave not only the multiplicity as a function of sum energy slices, but also the widths of the multiplicity distributions, as also shown in Fig. 9. Substitution of a Ge counter for the sum spectrometer permitted determination of the average multiplicities and widths for the 4n, 5n, and 6n reaction channels, which are also plotted. Finally, use of the Ge counter in coincidence with the sum spectrometer

gave the summed-energy distribution for each of the reaction products, as shown in Fig. 9(top). Also it can be seen that the multiplicities in Fig. 9 reach quite high values. In fact, these are the highest multiplicities yet isolated and observed by any method for a compound nucleus reaction.

Perhaps the greatest value of the use of the sum spectrometer is that the effects of relatively small changes in the angular momentum can be determined. For example, Fig. 10 shows the 0° NaI spectra from the $^{124}Sn + ^{40}Ar \rightarrow ^{164}Er^*$ system in coincidence with 3 MeV-wide slices of summed energy, normalized to the number of transitions per event per 200 keV. Initially the height in the most intense channels (500-600 keV) increases, but beyond slice 5 this stops and the upper edge of the bump moves to higher energy. This is the expected rotational behavior for these deformed Er product nuclei, with the additional transitions of higher spin also being of higher energy. By subtracting the spectrum of one slice from the next, we obtain the curves in Fig. 10(bottom), which show the very regular behavior of the additional transitions up to slice 8. If we integrate the difference spectrum for slice 7-slice 6, and take its centroid, we find 3.4 transitions were added having an average energy of 1.40 MeV. Similarly, slice 6-slice 5 gives 4.0 transitions with an average energy of 1.20 MeV. From the difference in energy, 0.20 MeV, and the average number of transitions, 3.7, we determine the moment of inertia to be $2\mathcal{J}/\hbar^2 = 150\ \mathrm{MeV}^{-1}$ for $E_\gamma = 1.30$ MeV. These values correspond to a spin of about 50 $\hbar$, and this is for states at the top of slice 6. This is surely the simplest and clearest view we have had yet about the transitions at such spins in any nucleus.

Much more can be said about the information available from the use of the sum spectrometer and the other techniques mentioned, and this will be done by the speakers that follow. I have purposely not discussed determinations of the entry line and the neutron-drip line and a number of other such topics, not because I meant to slight them, but because of the limits of time and because they will either be discussed by others

or are included in a number of excellent contributed papers. But the excitement, health, and vigor of continuum γ-ray studies will be evident from such work, and we are clearly coming to have a much better knowledge of very high-spin states as we develop better research tools. A whole new spectroscopy of high-spin states awaits us if we are only clever enough to find the proper methods of investigation.

Acknowledgments: A large number of very capable and congenial visitors contributed to the work described; during the past three years these included Drs. M. M. Aleonard, P. Aguer, R. Bauer, Th. Byrski, M. V. Banaschik, M. A. Deleplanque, Y. El Masri, C. Ellegaard, D. Fossan, D. Habs, H. Hübel, B. Herskind, D. Hillis, H. J. Körner, I. Y. Lee, J. O. Newton, M. Neiman, C. Roulet, R. S. Simon, and U. Smilansky. I am greatly indebted to F. S. Stephens for many discussions on all aspects of this subject.

This work was carried out under the auspices of the Nuclear Physics Division of the U.S. Department of Energy.

REFERENCES

1. S.Cohen, F.Plasil, and W.J.Swiatecki, Ann. Phys. 82, 557 (1974).
2. J.O.Newton, I.Y.Lee, R.S.Simon, M.M.Aleonard, Y.El Masri, F.S. Stephens, and R.M.Diamond, Phys. Rev. Lett. 38, 810 (1977).
3. A.Bohr and B.Mottelson, Phys. Rev. 89, 316 (1953) and Phys. Rev. 90, 717 (1953).
4. A.Bohr and B.Mottelson, Nuclear Structure, Vol. II, Chapter 4 (W.A.Benjamin, Inc., Reading, Massachusetts, 1975).
5.(a) T.L.Khoo, R.K.Smither, B.Haas, O.Häusser, H.R.Andrews, O.Horn, and D.Ward, Phys. Rev. Lett. 41, 1027 (1978).
5.(b) C.Baktash, E.der Mateosian, O.C.Kistner, and A.W.Sunyar, Phys. Rev. Lett. 42, 637 (1979).
6. D.Horn, O.Häusser, T.Faestermann, A.B.McDonald, T.K.Alexander, J.R.Beene, and C.J.Herrlander, Phys. Rev. Lett. 39, 389 (1977).
7. R.S.Simon, M.V.Banaschik, R.M.Diamond, J.O.Newton, and F.S.Stephens, Nucl. Phys. A290, 253 (1977).

8. S.J.Feenstra, J.van Klinken, J.P.Pijn, R.Janssens, C.Michel, J.Steyaert, J.Vervier, K.Cornelis, M.Huyse, and G.Lhersonneau, Phys. Lett. 80B, 183 (1979); S.J.Feenstra, W.J.Ockels, J.van Klinken, M.J.A.De Voigt, and Z.Sujkowski, Phys. Lett. 69B, 403 (1977).

9. M.A.Deleplanque, I.Y.Lee, F.S.Stephens, R.M.Diamond, and M.M.Aleonard, Phys. Rev. Lett. 40, 629 (1978).

10. H.Hübel, U.Smilansky, R.M.Diamond, F.S.Stephens, and B.Herskind, Phys. Rev. Lett. 41, 791 (1978).

11. P.O.Tjøm, I.Espe, G.B.Hagemann, B.Herskind, and D.Hillis, Phys. Lett. 72B, 439 (1978).

12. F.S.Stephens, P.Aguer, C.Ellegaard, D.Fossan, D.Habs, D.Hillis, H.J.Körner, C.Roulet, and R.M.Diamond, to be published.

FIGURE CAPTIONS

Fig. 1. Angular momentum at which fission barrier becomes zero (solid line) or 8 MeV (dashed line) as a function of mass number. The stable shape is oblate below ℓ_I and triaxial between ℓ_I and ℓ_{II} [Ref. 1].

Fig. 2. Moments of inertia and rotational energies for oblate and prolate shapes with rotation around and perpendicular to the symmetry axis.

Fig. 3. Gamma-ray de-excitation routes following heavy-ion compound-nucleus reactions [Ref. 7].

Fig. 4. The raw (squares) and normalized unfolded (small black dots) continuum γ-ray spectrum from the reaction $^{126}Te(^{40}Ar,4n)^{162}Yb$ at 181 MeV. The larger dots are five-channel averages. At the top is the 0°/90° ratio for the unfolded spectra. At the bottom are schematic unfolded spectra for the same case (solid line) and for the reactions $^{80}Se(^{86}Kr,4n)^{162}Yb$ at 331 MeV (dotted line), $^{126}Te(^{40}Ar,4n)^{162}Yb$ at 157 MeV (larger-dashed line), and $^{150}Sm(^{16}O,4n)^{162}Yb$ at 87 MeV (shorter-dashed line) [Ref. 7].

Fig. 5. Schematic representation of Yb continuum spectra following ^{40}Ar reactions. The 5n and 4n channels at 181 MeV correspond to similar angular momenta as the 4n and 3n channels at 157 MeV [Ref. 7].

Fig. 6. Measured conversion-electron coefficients, α_T, for the 4n reaction (circles) compared with theoretical E1, E2, and M1 values (curves) and with coefficients obtained with open gate on coincident Ge counter [Ref. 8].

Fig. 7. Experimental (left) and calculated (right) multiplicity spectra for the systems and bombarding energies indicated. One γ-ray spectrum is also shown at the top for each system [Ref. 9].

Fig. 8. (a) Sum of two-fold to six-fold coincidence γ-ray spectra (raw pulse-height data) measured at 0° for a self-supporting ^{27}Al target (solid curve) and for a ^{27}Al target on Au backing (dotted curve). (b) Ratio of those two spectra. (c) Ratio of the unfolded spectra. The solid curve represents the best fit of the calculated ratio to the data. The dashed lines show the ratios calculated for the two extreme values of Q_o allowed by the experimental errors. (d) Same as in (b), but for ^{28}Si targets leading to $^{164}Er^*$ [Ref. 10].

Fig. 9. (Top) Total γ-ray energy for 4n, 5n, 6n, and 7n channels individually, and total sum spectrum. (Bottom) Multiplicity and multiplicity width (σ_M) vs. total γ-ray energy for 3 MeV wide slices in the total γ-ray energy. The solid triangles are average values of M_γ calculated for the indicated reaction channels at the centroid of the energy spectrum in the upper figure.

Fig. 10. (Top) Number of transitions per 200 keV per event for consecutive 3 MeV wide slices of the total γ-ray energy spectrum at the top of Fig. 9. Note how the yrast bump edge moves to higher energy from slice 4 to 7. (Bottom) The difference in spectra from neighboring slices as indicated in the figure.

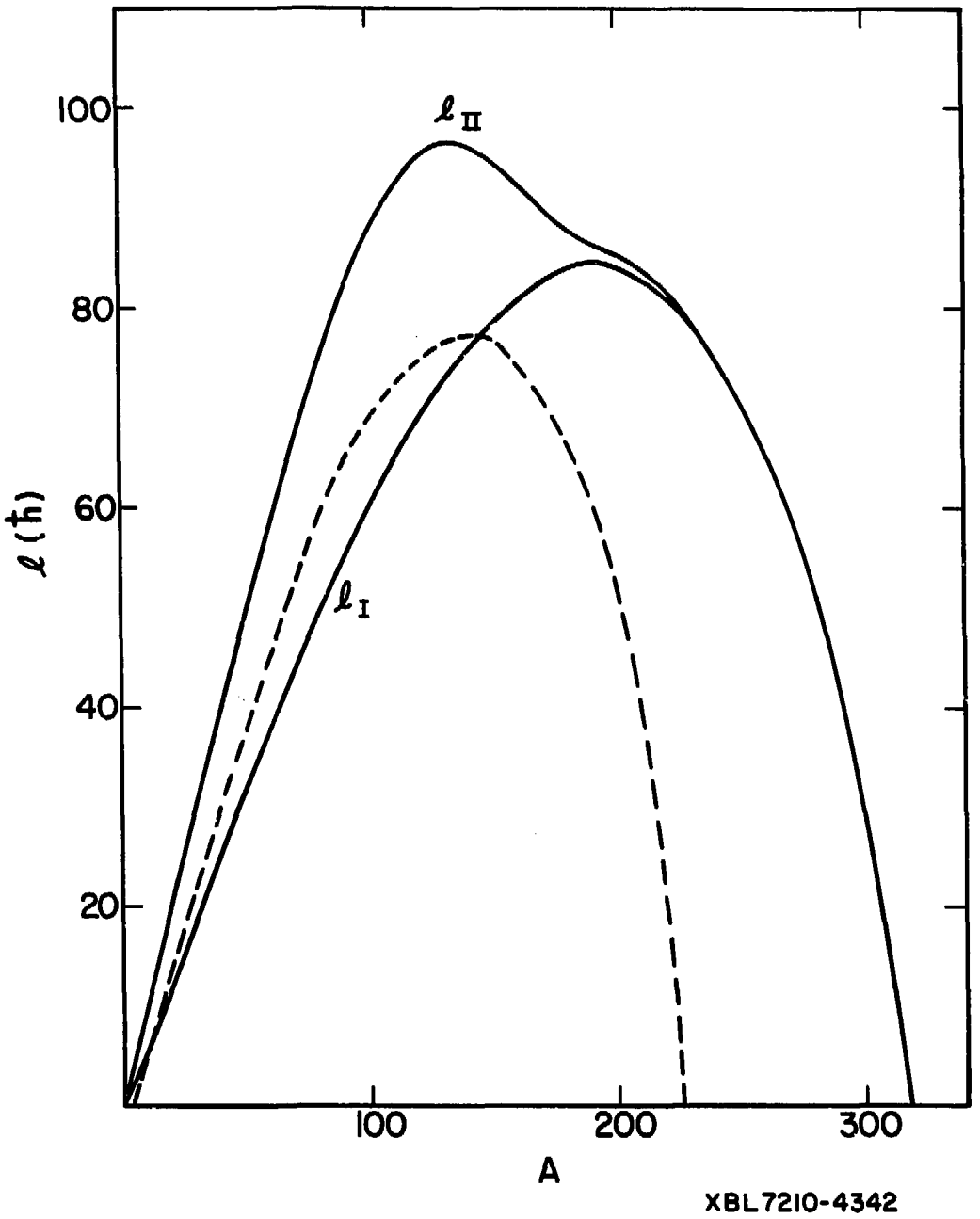

Fig. 1.

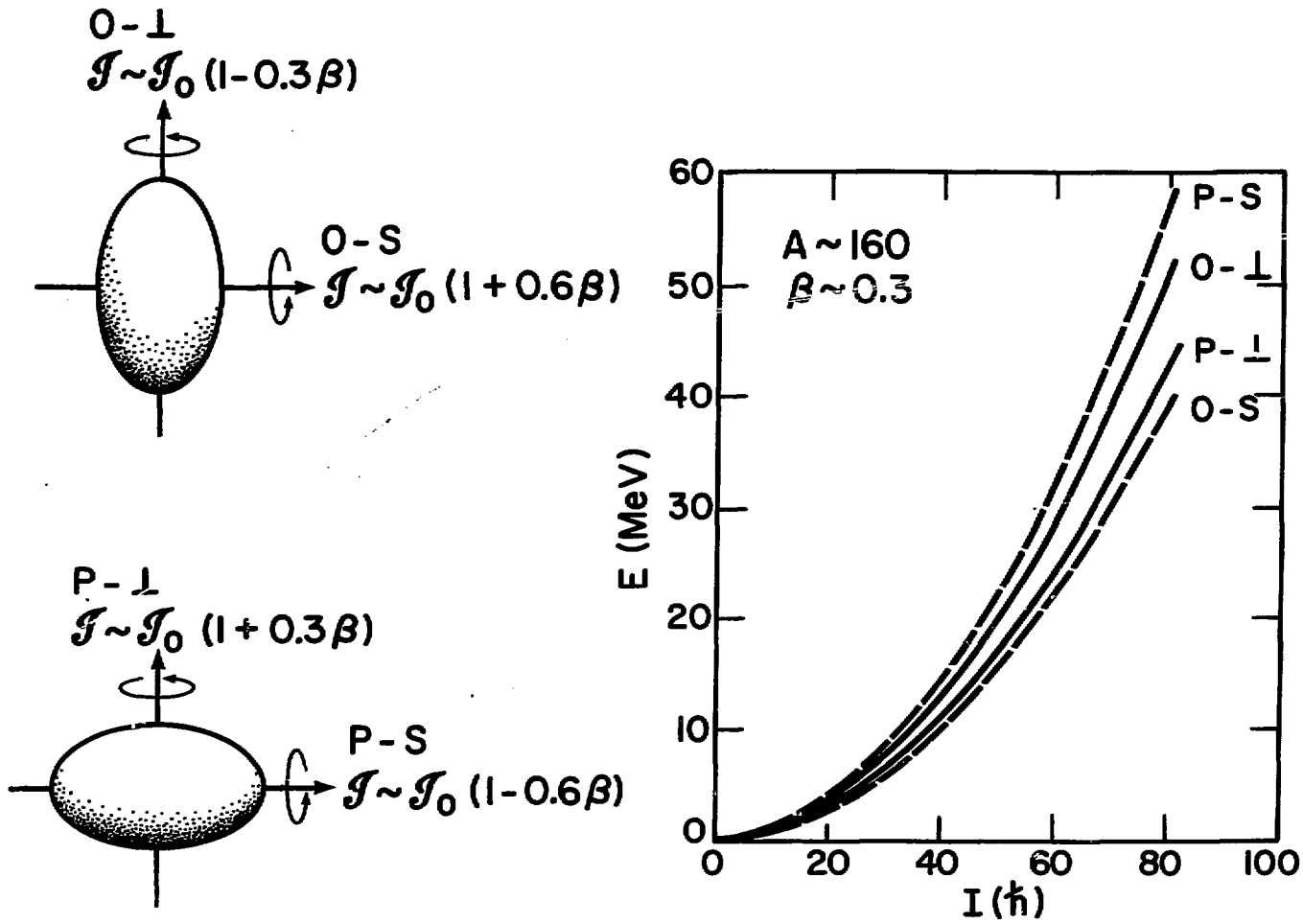

XBL 778-1649A

Fig. 2.

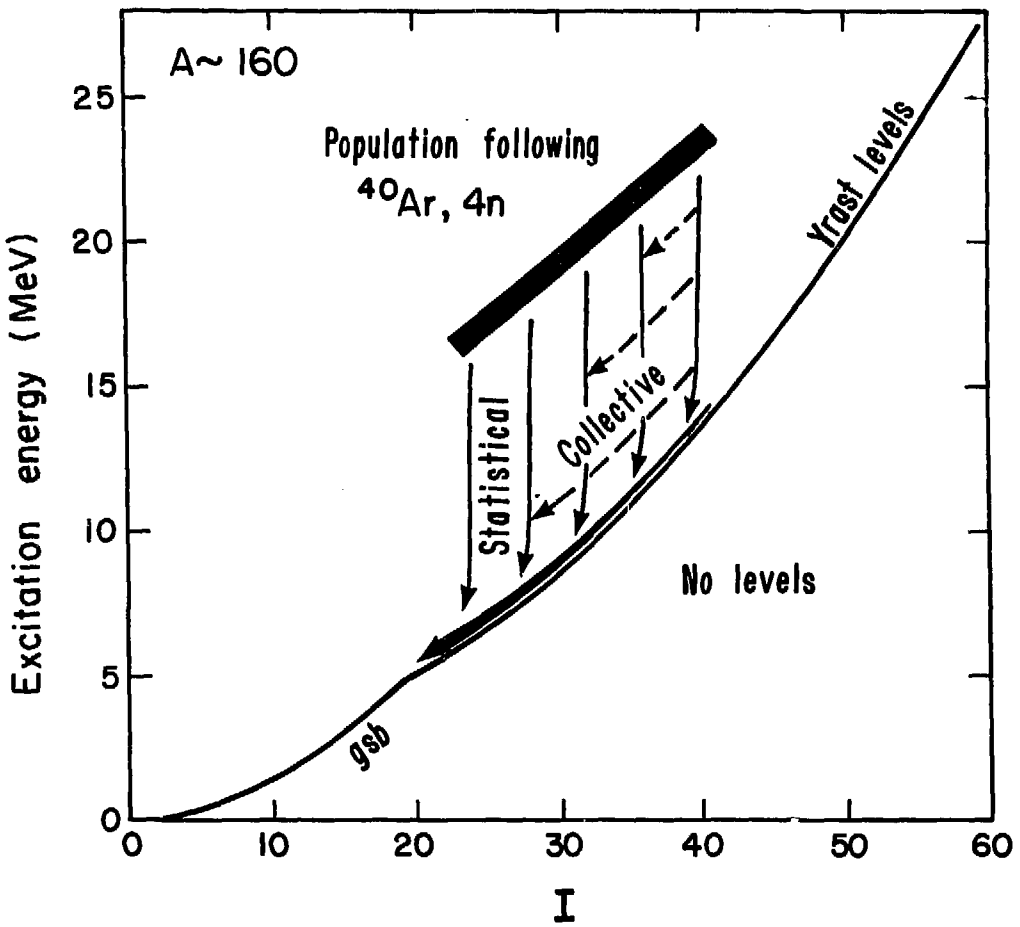

XBL 771-156

Fig. 3.

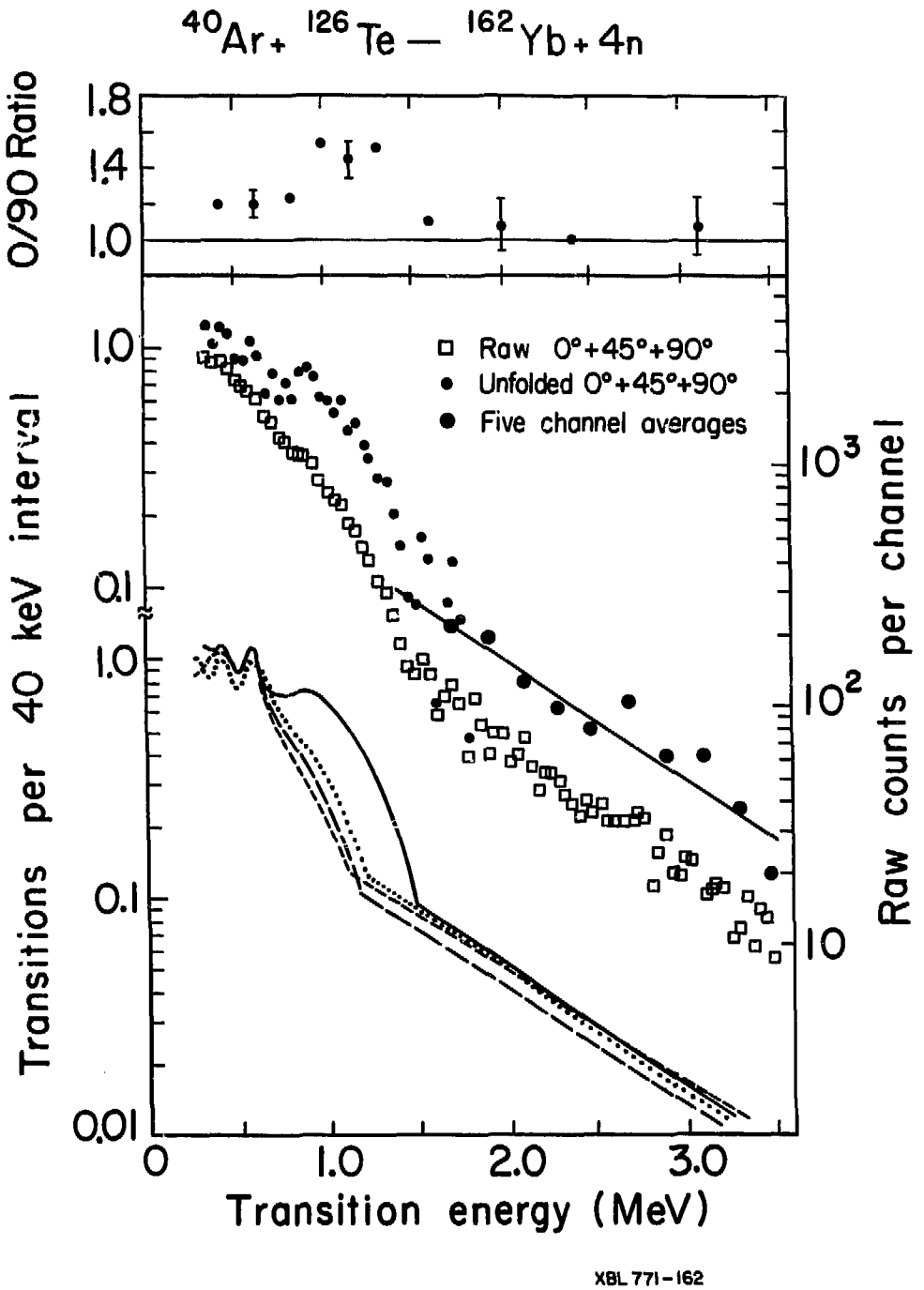
$^{40}Ar + ^{126}Te - ^{162}Yb + 4n$
0/90 Ratio
1.8
1.4
1.0
Raw 0°+45°+90°
Unfolded 0°+45°+90°
Five channel averages
Transitions per 40 keV interval
1.0
0.1
1.0
0.1
0.01
Raw counts per channel
10^3
10^2
10
0
1.0
2.0
3.0
Transition energy (MeV)
XBL 771-162

Fig. 4.

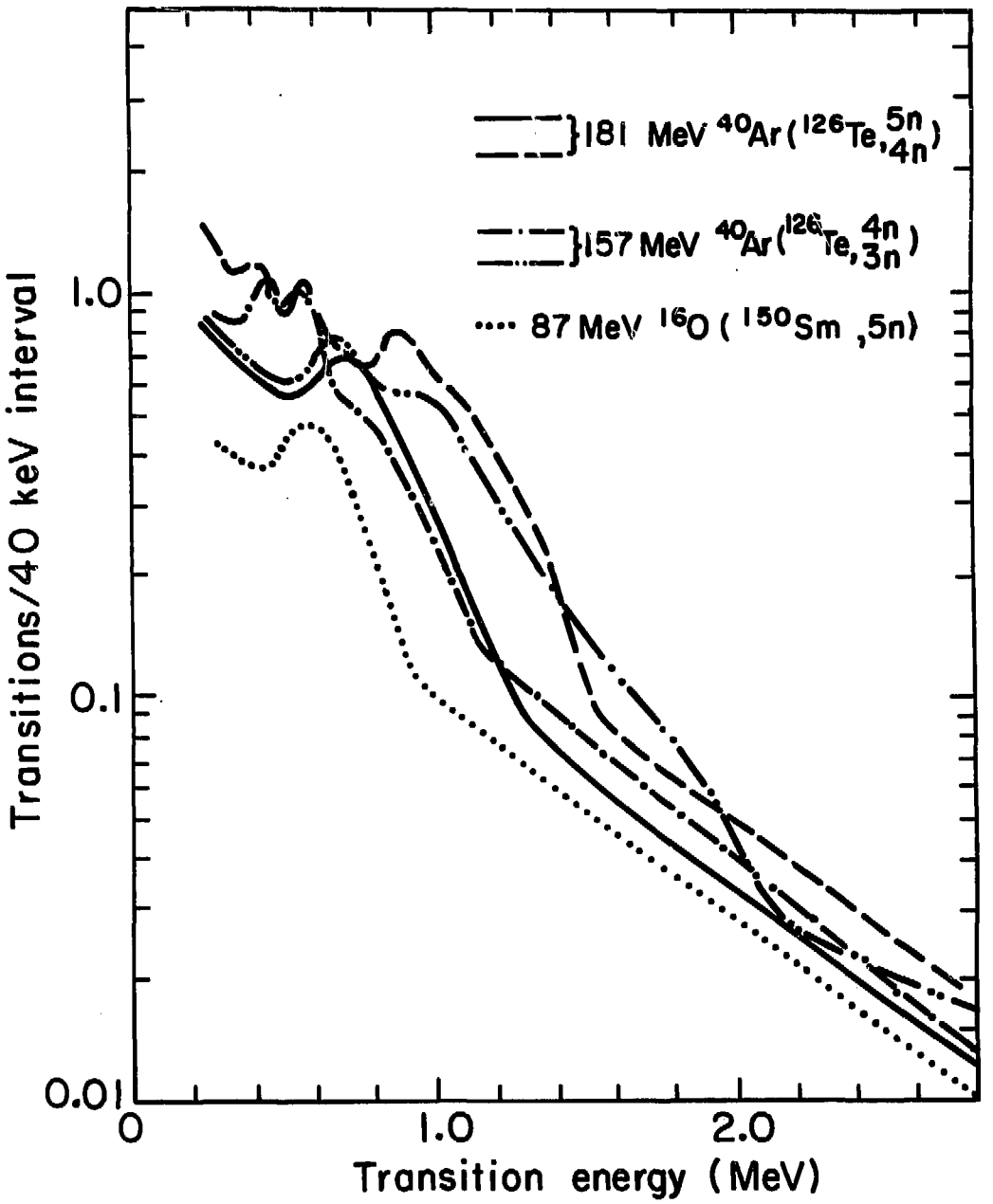

XBL 765-2848A

Fig. 5.

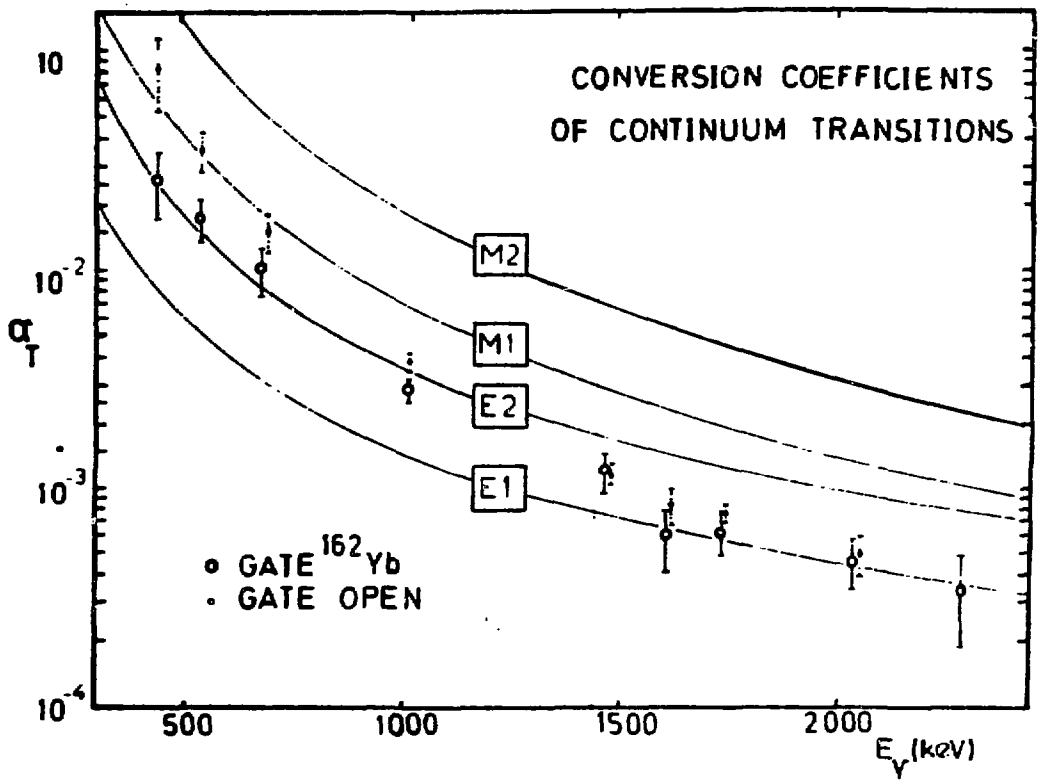

XBL 793-9005

Fig. 6.

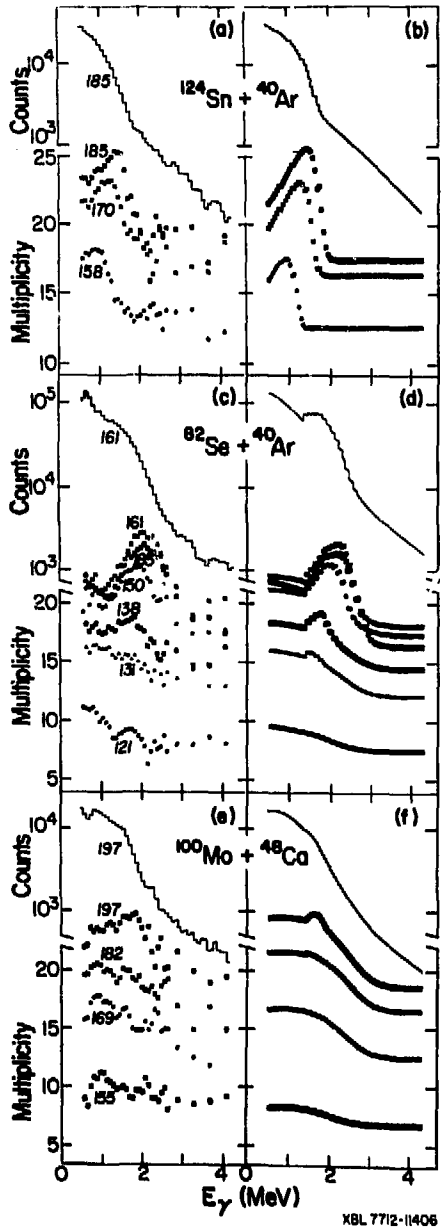
(a)
(b)
(c)
(d)
(e)
(f)
^{124}Sn + ^{40}Ar
^{82}Se + ^{40}Ar
^{100}Mo + ^{48}Ca
Counts
Multiplicity
185
170
158
161
150
138
131
121
197
182
169
155
E_γ (MeV)
XBL 7712-11406

Fig. 7.

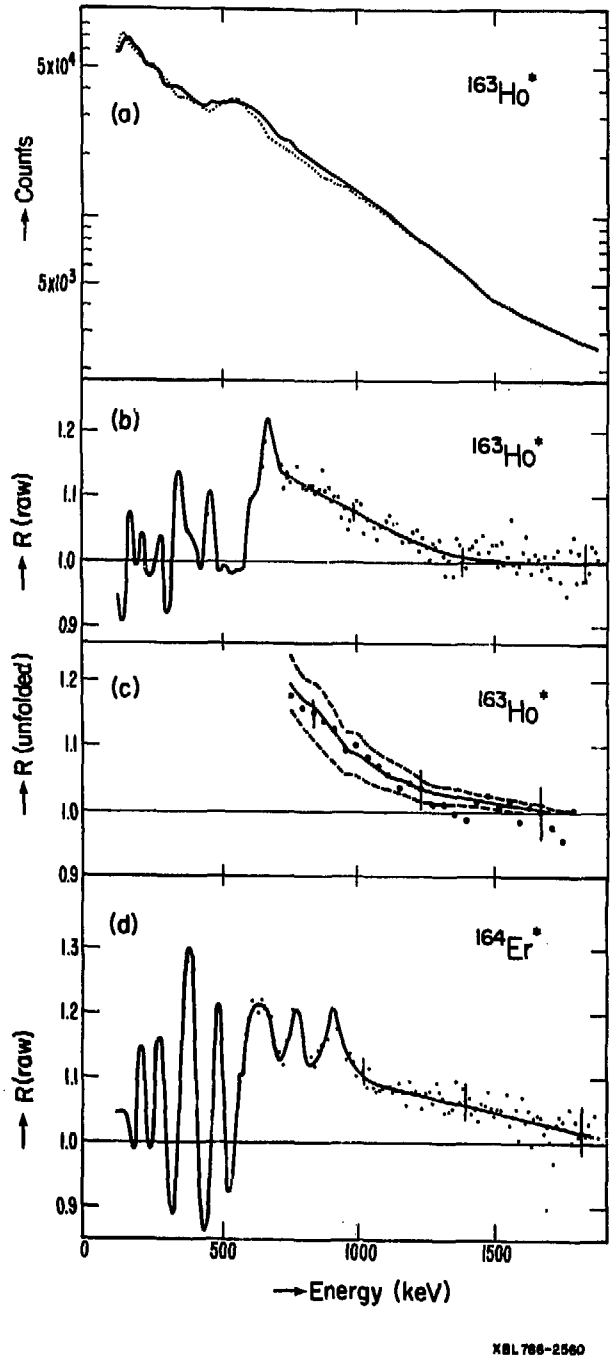
5x10⁴
5x10³
→ Counts
(a)
163Ho*
(b)
163Ho*
→ R (raw)
1.2
1.1
1.0
0.9
(c)
163Ho*
→ R (unfolded)
1.2
1.1
1.0
0.9
(d)
164Er*
→ R(raw)
1.3
1.2
1.1
1.0
0.9
0
500
1000
1500
→Energy (keV)
XBL 786-2560

Fig. 8.

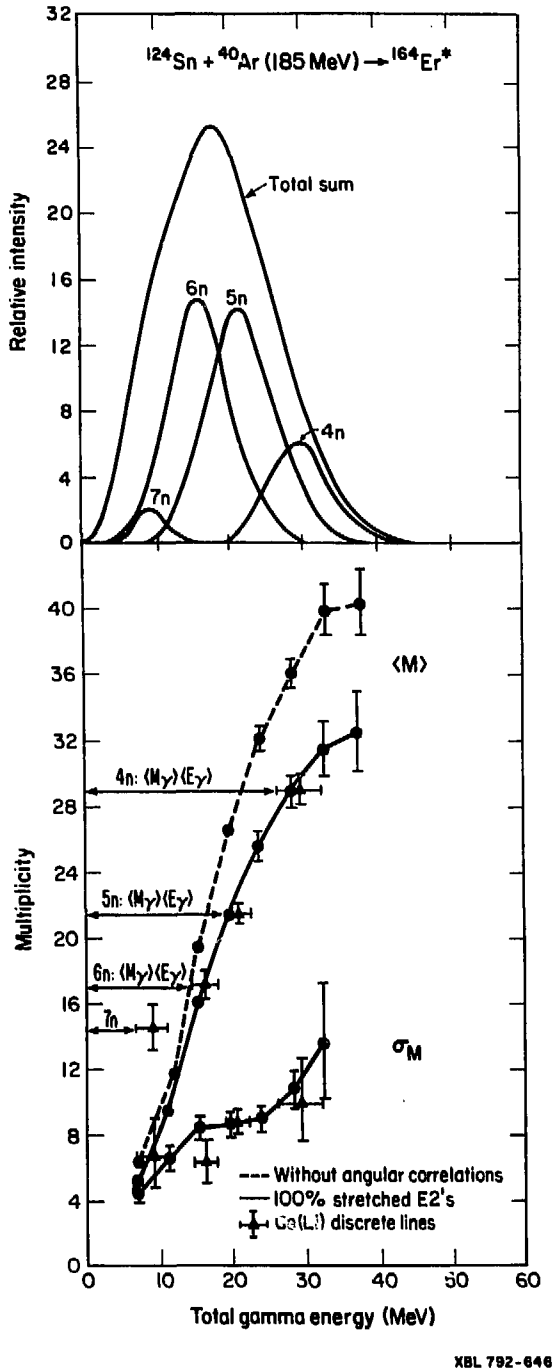
$^{124}Sn + ^{40}Ar$ (185 MeV) → $^{164}Er^*$
Total sum
6n
5n
4n
7n
Relative intensity
⟨M⟩
4n: ⟨Mγ⟩⟨Eγ⟩
5n: ⟨Mγ⟩⟨Eγ⟩
6n: ⟨Mγ⟩⟨Eγ⟩
7n
σ_M
Multiplicity
--- Without angular correlations
— 100% stretched E2's
Ge(Li) discrete lines
Total gamma energy (MeV)
XBL 792-646

Fig. 9.

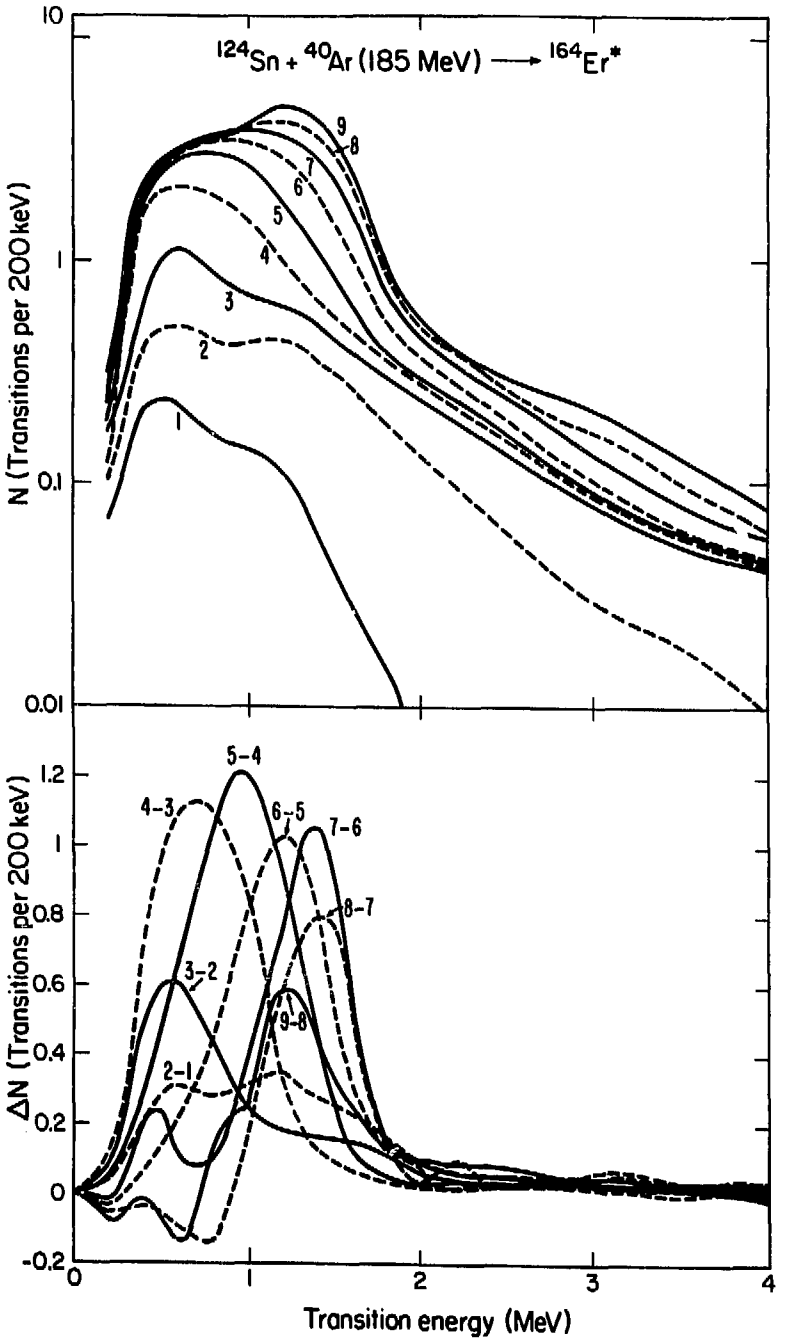

XBL 792-645

Fig. 10.

U.S.GPO:1979-689-058/(F)12